Giant planar Hall effect in epitaxial Fe_3O_4 thin films and its temperature dependence

A. Fernández-Pacheco,[1,2,4] J. M. De Teresa,[2,4,*] J. Orna,[1,2,4] L. Morellon,[1,2,4] P. A. Algarabel,[2,4] J. A. Pardo,[1,3] M. R. Ibarra,[1,2,4] C. Magen,[5] and E. Snoeck[5]

[1]*Instituto de Nanociencia de Aragón, Facultad de Ciencias, Universidad de Zaragoza, Zaragoza 50009, Spain*

[2]*Instituto de Ciencia de Materiales de Aragón, Facultad de Ciencias, Universidad de Zaragoza–CSIC, Zaragoza 50009, Spain*

[3]*Departamento de Ciencia y Tecnología de Materiales y Fluidos, Universidad de Zaragoza, Zaragoza 50018, Spain*

[4]*Departamento de Física de la Materia Condensada, Universidad de Zaragoza, Zaragoza 50009, Spain*

[5]*CEMES–CNRS/Nanomat, 29 Rue Jeanne Marvig, 31055 Toulouse Cedex 4, France*

(Received 28 May 2008; revised manuscript received 30 September 2008; published 2 December 2008)

We have investigated the giant planar Hall effect (ρ_{xy}) in epitaxial thin films of Fe_3O_4 grown on MgO (001) substrates with thickness ranging from 5 to 150 nm. A record value at room temperature of $|\rho_{xy}| \approx 60\ \mu\Omega$ cm was obtained for the 5-nm-thick film. Below room temperature, $|\rho_{xy}|$ shows a huge enhancement when crossing the Verwey transition, reaching the value of 16 mΩ cm at $T=73$ K for the 20-nm-thick film. This work demonstrates the potentiality of the planar Hall effect in magnetite thin films for studies of magnetization processes as well as for sensitive low-field detection. The influence of the superparamagnetic tendency for the thinnest films is highlighted. The results are also discussed in the context of fundamental aspects of Fe_3O_4 below the Verwey transition.

DOI: 10.1103/PhysRevB.78.212402 PACS number(s): 75.47.−m, 73.50.−h, 72.25.−b

The planar Hall effect (PHE) in magnetic materials occurs due to the difference in resistivity when the current and the magnetization are parallel ($\rho_\parallel$) or perpendicular ($\rho_\perp$) to each other, the physical origin being the same as the anisotropic magnetoresistance (AMR).[1] In the geometry of measurement of the PHE, both the magnetic field and the current are applied in the film plane. This is in contrast to the standard Hall effect where the magnetic field is applied perpendicular to the film plane and the physical origin is different.[1] In a simple but common situation with a single-domain sample showing in-plane magnetization (**M**), when a current density **J** is applied along the x direction and **M** forms an angle θ with the x direction, an electric field appears given by

$$E_x = J\rho_\perp + J(\rho_\parallel - \rho_\perp)\cos^2\theta, \tag{1}$$

$$E_y = J(\rho_\parallel - \rho_\perp)\sin\theta\cos\theta. \tag{2}$$

The longitudinal component of this electrical field gives rise to the AMR effect with resistivity $\rho_{xx}=E_x/J$, whereas its transversal component gives rise to the PHE effect, $\rho_{xy}=E_y/J$.

Due to the link between the magnetization direction and the PHE, the PHE has been used in thin films as a sensitive tool to study in-plane magnetization processes when transport measurements are more suitable than direct measurements of the magnetization.[2,3] The PHE can be also used for sensing low magnetic fields, showing advantages with respect to AMR sensors in terms of thermal drift.[4,5] Recently, the discovery of the so-called giant planar Hall effect (GPHE) found in the ferromagnetic semiconductor $(Ga_{1-x}Mn_x)As$ (Ref. 6) has attracted much interest. The effect at liquid helium temperature for this compound is 4 orders of magnitude higher than the existing in ferromagnetic metals, reaching values for ρ_{xy} of a few mΩ cm. The discovery has resulted in a thorough study of the magnetization properties of the material by means of this effect[7–9] and as a tool to investigate the resistivity of an individual domain wall.[10] The system $(Ga_{1-x}Mn_x)As$, with T_C below 160 K, is restricted for applications of the GPHE in magnetic sensing at low temperatures. In the search for giant PHE at room temperature, promising results have been found in Fe_3O_4 (Refs. 11 and 12) and manganites.[13,14] In these films, Bason *et al.*[12–14] proposed the use of PHE-based magnetic random access memory (MRAM) devices as an alternative to a more established magnetic tunnel junction (MTJ)-based technology. In the present work we address ourselves to explore the giant PHE in epitaxial Fe_3O_4 films in a wide range of film thicknesses and temperatures. At room temperature the PHE has been studied in films with thicknesses 5, 9, 15, 40, and 150 nm. The dependence of the PHE with temperature (down to 70 K) for 20-nm-thick and 40-nm-thick thin films has also been studied.

The Fe_3O_4 films were grown on MgO (001) substrates by pulsed laser deposition in an ultrahigh vacuum system with a background pressure of 5×10^{-9} torr. The exhaustive structural and magnetic characterizations indicate a 001-oriented epitaxial growth as well as a high crystallinity of the films. For details see Refs. 15 and 16. Film thickness was determined by x-ray reflectivity within a $\pm0.2\%$ estimated accuracy. Electrical transport measurements at room temperature were done in square (5×5 mm^2) samples in the Van-der-Pauw geometry. For measurements as a function of temperature a two-step lithography process was made to define a Hall geometry (width=300 μm) which minimizes transversal voltage offsets, really appreciable below the Verwey transition.[16] The optical lithography process was done so that the current was injected in the [100] direction, whereas $\mathbf{J}\parallel[110]$ for the samples measured at room temperature. To eliminate the possible thermal potentials from the measurements, as well as sample heating, we used the delta mode available in a 6220 dc source, 2182 A nanovoltmeter combined Keithley system. A closed-cycle refrigerator that permits varying the temperature from 300 to 10 K was used together with an electromagnet delivering fields up to 11 kOe.

The longitudinal resistivity (ρ_{xx}) values at room temperature for the selected films are listed in Table I. These are

TABLE I. Longitudinal (ρ_{xx}) and transversal (ρ_{xy}) resistivities (at maximum field) for the studied thin films at room temperature. Measurements were done with **J** applied in the [110] direction. The values for the transversal resistivity are obtained with $\theta=45°$.

Thickness (nm)	150	40	15	9	5
ρ_{xx}(mΩ cm)	5.5	7.0	12.4	23.4	121.4
ρ_{xy} at 11 kOe ($\mu\Omega$ cm)	−4.5	−8.3	−12.9	−15.3	−59.4
AMR(%)$=200\rho_{xy}/\rho_{xx}$	−0.18	−0.24	−0.21	−0.13	−0.1

comparable to other studies,[17–20] confirming the high quality of the films. The resistivity enhancement as the films get thinner is a direct consequence of the increase in the density of antiphase boundaries (APBs). APBs are structural defects formed during the growth process, which are unavoidably present when growing Fe_3O_4 epitaxial thin films regardless of the chosen substrate.[17–20] These defects entail important changes in the magnetic and transport measurements in comparison with the bulk material.[17–22] This is clearly observed in Fig. 1(a), where the conductivity is shown as a function of $t^{-0.5}$ (where t is the film thickness). The conductivity decreases as the film thickness is diminished following the model proposed by Eerenstein *et al.*[18] due to the dependence of the APB density with the film thickness. The fit to such a model is excellent as can be observed in Fig. 1(a) and the following parameters are extracted: the bulk conductivity $\sigma_{bulk}=235(3)\ \Omega^{-1}\,cm^{-1}$ (close to the bulk single-crystal value, $250\ \Omega^{-1}\,cm^{-1}$), the boundary conductivity $\sigma_{APB}=1.0(4)\ \Omega^{-1}\,cm^{-1}$ (theoretically $\sigma_{APB}=0$), and the boundary width $d=2.62(6)$ nm, in good agreement with results in molecular-beam-epitaxy-grown samples.[18] Direct visualization of the APB network in our samples has been obtained through transmission electron microscopy (TEM) measurements in plane-view samples. The experiments were carried out in a Philips CM30 LaB_6 microscope with a point resolution of 0.19 nm. Plane-view TEM specimens were prepared by mechanical thinning and ion polishing in a commercial precision ion polishing system (PIPS). The inset of Fig. 1(a) shows the dark field image of a plane-view TEM specimen (the 40 nm film) collected by selecting a (220)-type reflection after tilting the sample close to a two-beam condition, in which only the direct beam and one (220)-type reflection are strongly excited near the [001] zone axis. As illustrated in the inset of Fig. 1(a), the phase shift induced by the APB in the (220) reflection gives rise to strong darker contrast where the APB is located. We have to take into account that in using this reflection, we only observe the APBs whose phase shift is out of the plane associated to the selected (220) reflection, which has been estimated between ~55% and 2/3 of the total.[17,18] We have derived the antiphase domain (APD) distribution by means of the linear intercept method.[17,18,22] In previous studies, an exponential law has been used[20] due to the existence of a significant amount of low-size APDs. In our case, the amount of APDs below 5 nm is negligible within the experimental resolution of the TEM images, and the experimental distribution can be successfully fitted by a logarithmic-normal function as shown in Fig. 1(b). The mean APD value obtained for this sample is 24.4 nm with a standard deviation of 13.9 nm. This average domain size is comparable to other reported results for this film thickness.[17]

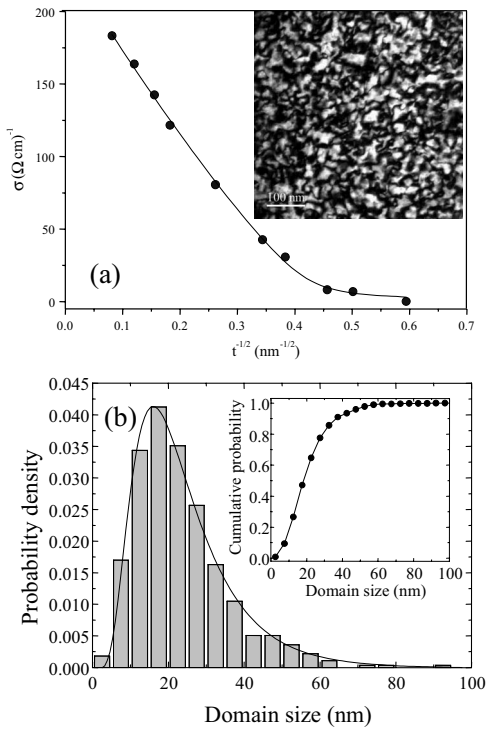

FIG. 1. (a) Experimental data (dots) of the value of conductivity as a function of $t^{-0.5}$, where t is the film thickness and the corresponding fit (line) to the model developed in Ref. 18. The inset shows a TEM planar-view image of the 40-nm-thick film where the APB network can be observed. The (220)-type reflection has been selected close to a two-beam condition, in which only the direct beam and one (220)-type reflection are strongly excited, near the [001] zone axis. (b) Size distribution of the antiphase domain size as calculated from the TEM image shown in (a) and the corresponding fit to a logarithmic-normal distribution. In the inset, the cumulative probability is shown as a function of the domain size.

For the study of the PHE, measurements were done with the applied magnetic field forming a fixed angle with the current, $\theta=45°$, since the signal will be maximum in this geometry when saturation in magnetization is reached [Eq. (2)]. To confirm that the even response measured was caused by the PHE, we also measured it with a 135° configuration. After subtracting the common offset, signals with opposite sign were obtained [see the particular case for the 40-nm-thick film at room temperature in the inset of Fig. 2(a)]. In Fig. 2(a) the results of the PHE for the 40-nm-thick film with current applied in two different directions, $\mathbf{J}\|[110]$ and $\mathbf{J}\|[100]$, are compared. The sign is different, which indicates that the AMR is positive ($\rho_{\|}>\rho_{\perp}$) if $\mathbf{J}\|[100]$, whereas it is negative ($\rho_{\|}<\rho_{\perp}$) if $\mathbf{J}\|[110]$. Such a difference in the sign of the AMR in Fe_3O_4 was explained by Ziese and Blythe[23] with a phenomenological model in which the AMR is expressed as a function of the magnetocrystalline anisotropy constants. As discussed in this reference, the AMR sign and absolute value have an intrinsic origin related to the spin-orbit coupling via the magnetocrystalline anisotropy constants. In Fig. 2(b) we show the transversal resistivity as a

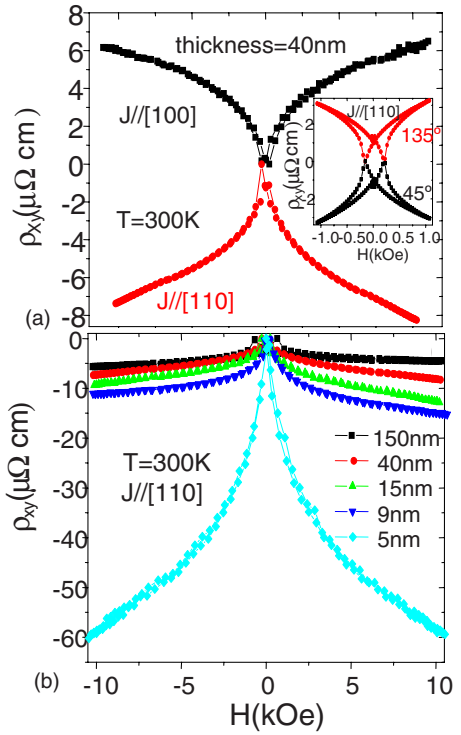

FIG. 2. (Color online) (a) Transversal resistivity as a function of the magnetic field for a 40-nm-thick film at room temperature. The magnetic field is applied forming $\theta=45°$ with current and two different current directions are compared, $\mathbf{J}\|[110]$ and $\mathbf{J}\|[100]$. In the inset, measurements with the magnetic field applied forming either $\theta=45°$ or $\theta=135°$ with current, $\mathbf{J}\|[110]$, are compared. The origin of the differences is discussed in the text. (b) Transversal resistivity as a function of the magnetic field ($\theta=45°$) for several thin-film thicknesses at room temperature with current direction $\mathbf{J}\|[110]$.

function of the applied magnetic field for all the studied thin films with $\mathbf{J}\|[110]$. The obtained values are of the same order as in Refs. 11 and 12 for Fe_3O_4, where 100 and 9 nm films were, respectively, studied. The values for ρ_{xy} at maximum field are listed in Table I, where a continuous decrease in magnitude with increasing film thickness is observed, as is the case for ρ_{xx}. The maximum value of $\rho_{xy}=-59.4$ $\mu\Omega$ cm is obtained for the 5-nm-thick film. A low-field slope of about 200 $\mu\Omega$ cm/T is found in this film, corresponding to a sensitivity of 400 V/A T, indeed a very large value.

An important issue to point out is the evolution of the films toward superparamagnetic (SP) behavior as the films decrease in thickness due to the reduction in the ferrimagnetic exchange coupling existing between spins surrounding the APBs.[18] The density of APBs varies as $t^{-1/2}$, where t is the thickness of the film.[17–20] The domains between antiphase boundaries for ultrathin films have sizes of a few unit cells and their magnetic moments start to fluctuate due to the thermal energy. The progressive shift toward zero field found for the peaks associated with the coercive field in our PHE measurements, as well as the increase in the slope for ρ_{xy} at high fields, suggests the occurrence of this phenomenon. These features influence the possible applications of the PHE observed in these films. The SP tendency is also reflected when the anisotropic magnetoresistance ratio [AMR $=100(\rho_{\|}-\rho_{\perp})/\rho_0$, with ρ_0 the resistivity at the coercive field]

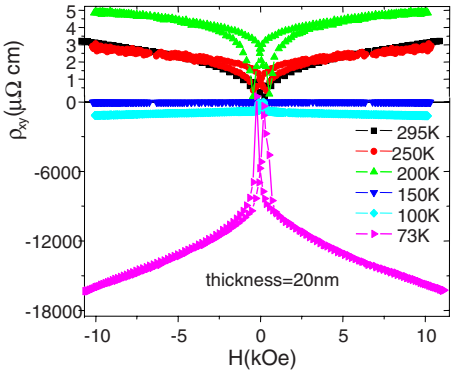

FIG. 3. (Color online) Transversal resistivity isotherms as a function of the magnetic field ($\theta=45°$) for a 20-nm-thick film. A change in sign for $T<150$ K is observed. Colossal values are found for $T<T_v$. Measurements have been done with $\mathbf{J}\|[100]$.

is calculated from PHE measurements (see Table I). The AMR has an approximately constant value of −0.2% for films above 10 nm, in agreement with bulk results and thin films in this range of thickness for $\mathbf{J}\|[110]$ (Ref. 23). Below 10 nm, an important decrease in magnitude occurs, compatible with the absence of anisotropy found for SP samples.[18] Magnetoresistance measurements (not shown here) corroborate this behavior. Thus, for very thin films (below 5 nm), the PHE will be limited in magnitude by the difficulty in magnetizing the sample and the decrease in the AMR value. Therefore, thinner films than the studied here are not expected to present higher PHE values than those reported ones. The difficulty to use the GPHE in very thin Fe_3O_4 films for magnetic storage should also be noticed since an improvement in signal magnitude with decreasing thickness also implies a decrease in coercive field. On the other hand, the superparamagnetic tendency implies a less hysteretical GPHE effect, which is welcomed for magnetic sensing.

In order to study the evolution of the GPHE as a function of temperature we have selected the 20-nm-thick and 40-nm-thick samples. From resistivity measurements, the Verwey transition takes place at a temperature (T_v) of 108 and 110 K, respectively. The transition in thin films is much less abrupt than in bulk samples and takes place at slightly lower temperatures, which can be explained by the suppression of long-range order in the octahedral iron sites due to the decrease in the domain size[18] or stress.[24] In Fig. 3 we show the ρ_{xy} isotherms from room temperature down to 70 K for the 20-nm-thick film. The longitudinal offset makes unfeasible measurements at lower temperatures. ρ_{xy} increases moderately when cooling from room temperature down to 200 K, changing its sign at about 150 K. When approaching the Verwey transition, a huge increment in the magnitude of ρ_{xy} occurs, as is also observed in the longitudinal resistivity. *Colossal* values, 1 order of magnitude bigger than the highest reported previously at 4.2 K in $(Ga_{1-x}Mn_x)As$ (Ref. 6), are found for $T<T_v$. Thus, ρ_{xy} is about 16 mΩ cm at $T=73$ K in this film. In the case of the 40-nm-thick film, two changes in sign are observed between room temperature and 70 K. A huge increment in the absolute value of ρ_{xy} is also observed when crossing T_v, giving, as a result, ρ_{xy} equal to about 15 mΩ cm at $T=70$ K. In order to gain more insight into

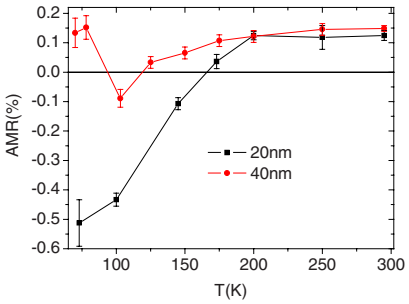

FIG. 4. (Color online) AMR ratio as a function of temperature for 20-nm-thick and 40-nm-thick films at 11 kOe. The AMR ratio is calculated from PHE measurements at 45° [$\mathrm{AMR}=100(\rho_{\parallel}-\rho_{\perp})/\rho_0=200\rho_{xy}/\rho_0$]. Measurements have been done with $\mathbf{J}\|[100]$.

the mechanisms responsible for the dependence with temperature of the PHE, AMR ratios calculated from the PHE at 11 kOe in both samples are shown in Fig. 4. The obtained values are in agreement with previous studies for the AMR in magnetite thin films,[23] with $\mathbf{J}\|[100]$. For both films, $\mathrm{AMR}\approx 0.2\%$, independent of temperature, is found for temperatures above 150 K. Different tendencies are followed in each thin film below this temperature. Whereas in the case of the 20-nm-thick film, a change in sign occurs, giving as a result negative values for $T<150$ K, for the 40 nm film ρ_{xy} is positive except in the surroundings of T_v. The changes in sign in the AMR are likely related to intrinsic changes in the magnetocrystalline anisotropy in this temperature range as previously observed in bulk single crystals.[25] Such changes will dramatically modify the anisotropy constants, which correspondingly will vary the AMR or PHE value as demonstrated in the phenomenological model presented in Ref. 23. The magnetic anisotropy in these films is expected to depend strongly on the film thickness and detailed magnetic studies beyond the scope of the present Brief Report would be required to clarify the quantitative relationship between the magnetic anisotropy changes and the AMR or PHE.

One important result inferred from the obtained AMR temperature dependence is that the absolute value of the AMR is large below the Verwey transition. The ground state of Fe_3O_4 below the Verwey transition is still a matter of debate.[26] Recent experiments indicate that pure electrostatic models do not seem to be able to explain the ground state below the Verwey transition and the electron-lattice coupling must play a key role in order to stabilize it.[26] The large values of the AMR below the Verwey transition observed by us give evidence for a substantial magnetocrystalline anisotropy of the ground state caused by a significant spin-orbital coupling. This suggests that the claimed strong electron-lattice coupling could arise from a large spin-orbital coupling.

In summary, the thickness and temperature dependences of the giant planar Hall effect in epitaxial Fe_3O_4 thin films have been studied and explained as a consequence of the resistivity anisotropy, $\rho_{\parallel}-\rho_{\perp}$, which is also responsible for the anisotropic magnetoresistance effect. Samples with moderately high antiphase boundary density have shown higher planar Hall effect signals due to the induced increase in the absolute value of the resistivity anisotropy, making them interesting candidates for magnetic sensing and nonvolatile memories and for magnetization studies through transport measurements. A record value of the planar Hall effect at room temperature of $|\rho_{xy}|\approx 60\ \mu\Omega$ cm was obtained for the 5-nm-thick film. As a function of temperature the planar Hall effect increases in magnitude, reaching colossal values below the Verwey transition, in the range of a few $m\Omega$ cm. The anisotropic magnetoresistance values inferred from these measurements indicate that the ground state below the Verwey transition likely bears a substantial spin-orbit coupling.

Financial support from the Spanish Ministry of Science (through Projects No. MAT2005-05565-C02 and No. MAT2008-06567-C02 including FEDER funding), the ESF-THIOX project, and the Aragon Regional Government are acknowledged.

*deteresa@unizar.es

[1] I. A. Campbell and A. Fert, in *Ferromagnetic Materials*, edited by E. P. Wohlfarth (North-Holland, Amsterdam, 1982), Vol. 3, p. 747.
[2] G. Li *et al.*, Phys. Rev. B **65**, 134421 (2002).
[3] S. T. B. Goennenwein *et al.*, Appl. Phys. Lett. **90**, 142509 (2007).
[4] A. Schuhl, F. Nguyen Van Dau, and J. R. Childress, Appl. Phys. Lett. **66**, 2751 (1995).
[5] A. O. Adeyeye *et al.*, Sens. Actuators, A **116**, 95 (2004).
[6] H. X. Tang *et al.*, Phys. Rev. Lett. **90**, 107201 (2003).
[7] K. Y. Wang *et al.*, Phys. Rev. B **72**, 085201 (2005).
[8] W. L. Lim *et al.*, J. Appl. Phys. **99**, 08D505 (2006).
[9] D. Y. Shin *et al.*, IEEE Trans. Magn. **43**, 3025 (2007); Phys. Rev. Lett. **98**, 047201 (2007).
[10] H. X. Tang *et al.*, Nature (London) **431**, 52 (2004); H. X. Tang and M. L. Roukes, U.S. Patent No. 6,910,382 (2004).
[11] X. Jin *et al.*, J. Appl. Phys. **99**, 08C509 (2006).
[12] Y. Bason *et al.*, J. Appl. Phys. **101**, 09J507 (2007).
[13] Y. Bason *et al.*, Appl. Phys. Lett. **84**, 2593 (2004).
[14] Y. Bason *et al.*, J. Appl. Phys. **99**, 08R701 (2006).
[15] J. M. De Teresa *et al.*, Microelectron. Eng. **84**, 1660 (2007).
[16] A. Fernández-Pacheco *et al.*, Phys. Rev. B **77**, 100403(R) (2008).
[17] A. V. Ramos *et al.*, J. Appl. Phys. **100**, 103902 (2006).
[18] W. Eerenstein *et al.*, Phys. Rev. B **66**, 201101(R) (2002); W. Eerenstein, T. Hibma, and S. Celotto, *ibid.* **70**, 184404 (2004); S. Celotto, W. Eerenstein, and T. Hibma, Eur. Phys. J. B **36**, 271 (2003).
[19] S. K. Arora *et al.*, J. Appl. Phys. **100**, 073908 (2006).
[20] A. M. Bataille *et al.*, Phys. Rev. B **74**, 155438 (2006).
[21] D. T. Margulies *et al.*, Phys. Rev. B **53**, 9175 (1996); D. T. Margulies *et al.*, Phys. Rev. Lett. **79**, 5162 (1997).
[22] C. Magen *et al.*, J. Appl. Phys. **104**, 013913 (2008).
[23] M. Ziese and H. J. Blythe, J. Phys.: Condens. Matter **12**, 13 (2000).
[24] X. W. Li *et al.*, J. Appl. Phys. **83**, 7049 (1998).
[25] V. Skumryev *et al.*, J. Magn. Magn. Mater. **196-197**, 515 (1999).
[26] I. Leonov and A. N. Yaresko, J. Phys.: Condens. Matter **19**, 021001 (2007).